Kossovich EL, Borodich FM, Bull SJ, Epshtein SA.

Substrate effects and evaluation of elastic moduli of components of inhomogeneous films by nanoindentation.

***Thin Solid Films* 2016, 619, 112–119.**

Substrate effects and evaluation of elastic moduli of components of inhomogeneous films by nanoindentation

F.M. Borodich [1*], **S.J. Bull**[2], **E.L. Kossovich**[3] and **S.A. Epshtein**[3]

[1] School of Engineering, Cardiff University, Cardiff CF24 3AA, UK

[2] School of Chemical Engineering and Advanced Materials, Newcastle University, Newcastle upon Tyne NE1 7RU, UK

[3] Laboratory of Physics and Chemistry of Coals, Mining Institute, National University of Science and Technology "MISiS", 119049, Leninsky pr.4, Moscow, Russia

[*] Corresponding author: e-mail: BorodichFM@cardiff.ac.uk

Abstract

Depth-sensing nanoindentation (DSNI) is a very popular technique that is used for evaluation of mechanical properties of both homogeneous thin films and bulk material samples. Recently it has been proposed by the authors to apply the DSNI to components of highly inhomogeneous materials that could contain pores and cracks. The extended techniques assume that the DSNI is applied to very thin films (the thickness is about 10–20 μm) of the tested inhomogeneous material glued to a transparent rigid substrate. The combination of DSNI and transmitted light microscopy allows us to visualize the regions of tested components. Because we study not a bulk material sample but rather a thin films glued to the substrate, the approximating functions have to be used to extract the real elastic modulus of the tested component. We present the results of evaluation of elastic moduli of coal samples at varying depth of maximal indentation using seven approximating functions. Comparing the experimental values with the results of approximations and calculating statistical characteristics such as the residual sum of squares and the coefficient of determination, it was found that the most appropriate are the exponential decay function and a function based on power-law approximation.

Key words: depth-sensing nanoindentation, mechanical characteristics, glue, substrate, coal films

1. Introduction

Methods of indentation are widely applied to a variety of problems of engineering and materials science [1,2]. Mainly these methods are used to evaluate mechanical characteristics of homogeneous and vertically inhomogeneous materials. For examples, the indentation techniques has been used in biomechanics for mechanical characterization of biological samples such as insect cuticle, plant cuticle and snake skin [3] or for characterization of the properties of bones [4], in civil engineering and geomechanics to evaluate elastic properties of coals, rocks and cementitious materials and ability of rocks to be destructed or for mechanical characterization of coals [5-13]. The information on the degree of inhomogeneity, structural composition, hardness and brittleness of components of the materials plays an important role in assessing strength, developing fracture models and estimation of other properties. For example, one needs to have this information in order to estimate ability of coals to oxidize and their toughness. If one knows mechanical characteristics and the specific geometric size of the material components then the behaviour of a heterogeneous material at meso- and macro-scales may be predicted by using methods of micromechanics of materials [14].

It is assumed often that many natural materials such, as bones, rocks and coals are generally considered as materials with relatively homogeneous properties. Hence, the mechanical characteristics are often studied by the microindentation techniques. For example, the applications of microindentation for evaluation of microhardness and microbrittleness of coals are reviewed in [9]. Despite the prevalence of the use of microindentation methods for determining such indicators as microhardness and microbrittleness, they are of little use for highly inhomogeneous materials such as many composite materials, rocks consisting of different minerals and coals consisting of many macerals due to specific features of their structure. Indeed, these materials are in fact, spatially inhomogeneous at both micro- and nanoscales [4, 11, 15]. In particular, coals are extremely complex heterogeneous materials that were formed by geological processes.

In view of the above, and because the microindentation methods do not allow researchers to assess the properties of components of essentially inhomogeneous materials, during the last two decades there were several attempts to employ DSNI methods for more accurate determination of mechanical characteristics of individual components of the cement pastes and other mixtures which are widely used in constructions [10-12]. We were able to find only a couple of papers where the DSNI was used to determine mechanical properties of rock minerals [12, 13]. The reasons for using the nanoindentation method for evaluating properties of cement pastes and rocks are similar: these materials are inhomogeneous at the micro-level, therefore, one needs to evaluate the mechanical properties of all constitutive components.

We would like to underline that the above studies were based on the use of relatively thick polished samples that could be well approximated as an elastic half-space, and the use of optical microscopy operating in reflected light. However, it is difficult to apply these approaches to spatially inhomogeneous materials whose components have similar colour in the reflected light. For example, one can see from Figure 1 that different groups of coal macerals are practically not distinguishable by optical microscopy operating in reflected light without immersion medium. Recently it has been proposed by the authors [15] to combine the DSNI techniques and transmitted light microscopy, and apply the techniques to very thin and very smooth polished sections (thin films) of the inhomogeneous materials. If the thickness of the film is about 10–20 μm and it is glued to a transparent rigid substrate then one can work using transmitted light. The use of such thin films enabled us to avoid the influence of pores and cracks and to visualize the regions of tested components in order to ensure that the regions belonging to the same specific maceral are tested. This in turn, allowed us to get maps of mechanical properties like hardness and elastic contact modulus of the tested area.

It should be noted that due to the influence of the glue layer and the glass substrate, the traditional methods of interpretation of test results within a depth-sensing nanoindentation method show effective characteristics of section/substrate system, rather than the properties of the material. Because we study not a bulk material sample but rather a thin films/glue system, the approximating functions have to be used to extract the real elastic modulus of the tested component.

The experiments were performed on two different macerals at varying depth of maximal indentation. We present here the results of evaluation of elastic moduli of the macerals using seven approximating functions. Comparing the experimental values with the results of approximations and calculating statistical characteristics such as the residual sum of squares and the coefficient of determination, we may decide what approximate functions are the most appropriate for description of the experiments and therefore, to find the true values of the elastic contact modulus.

2. Preliminaries

2.1. Depth-sensing nanoindentation.

The use of indentation techniques for mechanical characterization of materials has a long history (see, e.g. reviews [16, 17]). Development and implementation of a revolutionary new method of depth-sensing nanoindentation (DSNI), introduced by Kalei [18] under the supervision of M.M. Khrushchov in the Institute of Machines Science of USSR Academy of Sciences, significantly expanded the capabilities of determining physical and mechanical properties of the materials. As a part of this method, the diagrams are recorded for loading and unloading of the indenter in the test samples in terms of "force-depth of indentation" coordinates, i.e. the $P-h$ diagram is continuously monitored for load increase and decrease. Here, h is the depth of indentation (penetration of the indenter into the sample surface) and P is the force loading the indenter. A typical $P-h$ curve has usually two branches that do not coincide; at the loading regime the curve reflects both elastic and plastic deformation of the material, while the unloading regime occurs usually elastically.

It is interesting to note that the first Kalei's nanoindenter was based on a modifications of a standard PMT-3 microhardness tester developed by Khrushchov and Berkovich that was a Soviet analogue of Vickers indenter employing four-sided pyramidal diamond tip. The employment of the same PMT-3 device was included in the state standards [5] used in the Soviet Union and the standards that are currently valid in a number of the former Soviet Union (FSU) countries for characterization of microhardness of many materials, including metals and hard coals and for estimation of microbrittleness of hard coals. On the other hand, the first ever transmission electron microscopy studies of indents presented by Khrushchov and Berkovich [19] showed that the images of imprints of four-sided pyramidal tips are less sharp than imprints of three-sided pyramidal tips.

Methods of depth-sensing nanoindentation evolved very quickly and modern sensors can accurately control the load and the depth of the indentation at nanometers and micronewtons scale, respectively. Advances in depth-sensing nanoindentation made it possible to study a variety of homogeneous materials at very small volumes, for example, properties of samples with a thickness of only a few micrometers [20, 21].

Derivation of Bulychev-Alekhin-Shorshorov relation (BASh) [22] changed the indentation techniques and expanded the range of results obtained from the experiment. It was found that the use of the slope for the initial part of the unloading branch of the $P-h$ curve allows the

researchers to evaluate elastic contact modulus of "indentor-sample" pair, because for the elastic branch at unloading of the homogeneous half-space we have

$$S = dP/dh = 2E^* a \approx 2E^* \sqrt{A/\pi}\,. \qquad (1)$$

Here, S is the inclination of the displacement-load curve, a is the characteristic size of the contact zone, A is the area of the contact and E^* is a contact elastic modulus. The latter is determined as a combination of elastic moduli E_i and E_e and Poisson's ratios ν_i and ν_e for indentor (with index *i*) and sample (index *e*):

$$1/E^* = (1-\nu_e^2)/E_e + (1-\nu_i^2)/E_i\,. \qquad (2)$$

Although the use of the reduced contact elastic modulus E^* for sharp indenters (or pointed indenters [23]) is not mathematically justified (the Hertz approximation of a contacting solids as elastic half-spaces is violated in application to sharp indenters), currently (2) is employed in all models used by materials science community.

As it was noted by Galanov and his co-workers [24, 25], to analyse the unloading branch of the $P-h$ curve, one has to take into account not only the shift of the displacement axis due to a residual depth of plastic indentation but also the effective distance between the indenter and the imprint surfaces (this is the so-called Galanov effect or the effective shape effect). In addition, the BASh relation was derived for axisymmetric indenters, while actually the indenters are the pyramides and, hence (1) can be written as $S \approx 2\beta E^* \sqrt{A/\pi}$ where β is the correction factor for the indenter shape [3].

Further the BASh relation was derived under the assumption of elastic contact without friction between the indenter and the sample [22]. To estimate the influence of friction, the analogous contact problem was analysed under the assumption that the adhesion between the rigid indenter and an elastic sample is so strong that a contact occurs in the absence of any slip (the so-called no-slip boundary conditions). Borodich and Keer [26] showed that in this case we have

$$S = dP/dh = 2C_{NS}E^* a \approx 2C_{NS}E^* \sqrt{A/\pi}, \quad C_{NS} = (1-\nu_e)\ln(3-4\nu_e)/(1-2\nu_e)\,. \qquad (3)$$

Coefficient C_{NS} decreases from the value $C_{NS} = \ln 3 \cong 1.0986$ at $\nu_e = 0$ to $C_{NS} = 1$ at $\nu_e = 0.5$. Thus, it was shown, that the effect of friction on the results is rather insignificant. One can find an extended discussion related to connections between the Hertz-type contact problems and DSNI techniques in [27].

2.2. Elastic foundation models and approximating functions.

The above theoretical studies were developed in the framework of the Hertz contact theory [27]. However, the DSNI techniques are also used for studying of mechanical properties of the homogeneous materials covered by thin films (see, e.g. [20, 21]). It is clear that the inhomogeneity in such a ‘sample/substrate’ system is observed only in vertical direction, while the system is homogeneous horizontally.

It should be mentioned that the common procedures of nanoindentation could not be used directly for the investigation of components of a spatially inhomogeneous materials, in particular, components of rocks and coals. Therefore, one needs to modify the classical nanoindentation

procedures, in order to be able to study the properties of individual components of inhomogeneous materials. As it has been mentioned above, the authors have recently proposed a method of applying the depth-sensing nanoindentation to study horizontally inhomogeneous films [15]. The preliminary results of the studies were reported in [28]. Within the framework of the method, the inhomogeneous films are glued to a rigid transparent glass substrate. Hence, if the domain of a specific maceral is identified then the problem is reduced to well-known problem of identification of true characteristics of a thin film attached to an elastic substrate (a layer of a glue).

If one studies the thin film – elastic substrate system then conventional calculations [20, 29] give the value of the so-called effective (equivalent or composite) elastic modulus E_{eq}^{*}, while the purpose is to determine the value of a specific component of the inhomogeneous film (section) of the material E_{f}^{*}. Consideration of section/substrate complex as a film on an elastic foundation is considered to be classical. However, as it was mentioned by Kerr [30], the base is often an extremely difficult medium. In most cases, this problem can be reduced to relatively simple mathematical expressions that describe its reaction in the contact zone with a high degree of accuracy.

The simplest structural model of the elastic foundation is a Fuss-Winkler model, which considers a substrate as an elastic mattress with vertically arranged independent springs. A detailed overview of this and many other models of elastic fondations was presented by Kuznetsov in his book [31]. In particular, he discussed the models proposed by Wieghardt [32] and Filonenko-Borodich [33].

As Kuznetsov [31] noted, the vertical displacement of the elastic foundation $w(r)$ at point r, caused by pressure $p(\xi)$ acting at point ξ can be expressed as

$$w(x) = c\int p(\xi)K(x,\xi)d\xi,$$

where c is a constant determined from the elastic properties of the foundation, $K(x,\xi)$ is the kernel of the integral equation. Wieghardt [32] proposed an exponential shape of the kernel

$$K(x,\xi) = e^{-b|x-\xi|},$$

where b is a constant depending on characteristics of the elastic foundation, because $1/b$ is its characteristic depth of deflection. Kuznetsov [31] also noted that Wieghardt [32] offered no structural modelling for the elastic foundation contrary to Winkler interpreted the Fuss-Winkler model as a collection of vertical elastic springs. Filonenko-Borodich [33] introduced improvements to this structural model by adding some degree of spring dependence. Namely, he suggested to introduce a stretched elastic membrane exposed to constant stress field (tensions) T. Interaction between springs can be described by the intensity T of the aforementioned field. Denoting $\omega^2 = k/T$, where k is the spring constant, it is easy to show [31] that the Filonenko-Borodich structural model loaded by a concentrated force applied at the coordinate origin, can be described by the following expression

$$w(x) = e^{-\omega x}/(2T\omega),$$

which correlates well with the above expression under condition that the constants are taken as $c = (2T\omega)^{-1},\ b = \omega.$

Usually relations between an equivalent modulus and contact moduli of substrate (glue) E_s^* and sample E_f^* is expressed by

$$E_{eq}^*(x) = E_s^* + \left(E_f^* - E_s^*\right)\Phi(x) \ , \tag{4}$$

where $\Phi(x)$ is a weight function of relative penetration depth *x*. This function tends to zero at very high depth values and $\Phi(0) = 1$. For Vickers or Berkovich pyramidal indenters, the relative penetration depth can be determined either by means of an empirical relationship proposed by Oliver and Pharr (see, e.g. [20]), or as $x = a/t \approx \sqrt{24.5/\pi} \cdot h/t$, where t is the film thickness.

Thus, it is necessary to carry out additional tests with variable depth of maximum indentation and to evaluate the equivalent module for each depth. Further, in the paper we describe techniques for extracting the equivalent moduli of components of spatially inhomogeneous bodies and the results of application of the techniques for such highly inhomogeneous materials as coals. The values of equivalent moduli, extracted from the test with a variable depth of indentation, are compared with a variety of approximating functions proposed in the literature.

3. Materials and experimental methods

3.1. Features of coal samples.

We studied thin films (sections) of coals originated from the Donetsk and Kizel coal basins. We observed a significant difference in the petrographic composition of samples: the Kizel basin coals has liptinite macerals as dominating group (35%) and in the samples of coal from the Donetsk basin had dominating vitrinite group (up to 89%) with content of liptinite of 2%. At the same time, we observed a similar stage of metamorphism, the carbon percentage in all samples was about 88%. In addition, coal from the Kizel basin had a high content of hydrogen and sulphur.

3.2. Methods of thin coal sections preparation.

For the DSNI studies using optical microscopy operating in transmitted light, we prepared thin (around 13-14 microns) films of coals. The relatively thin coal samples of 25x25 mm size were impregnated in order to harden the interporous walls, and then their surface (perpendicular to flattening) was grounded sequentially and polished on automatic mineralogical complex RotoPol-35 by Struers (Denmark). The prepared sample was glued on a glass slide and stored in vacuum for several hours.

3.3. Methodology of nanoindentation experiments.

Formally, DSNI methods can be applied to relatively thick samples, as the basic requirements for the tests demand the sample to have a smooth and clean surface. However, use of very thin petrographic sections has several advantages. Indeed, under such condition we may confidently assume that: (i) the components of the material are presented along the entire thickness of the sample; (ii) the effects of pores and cracks during the indentation are practically removed; and (iii) thin coal films are transparent, therefore may be used for experiments with microscopes operating in transmitted light. This allows indentation in the domains occupied by the clearly visible component (maceral). Thus, we can more accurately assess the structure of the sample.

The experimental set-up was the same as described in Epshtein et al. [28], in which an automated nanoindentation system installed at the University of Newcastle was used for testing films having very smooth surfaces. The study was conducted in areas of clearly visible in transmitted light components localization (e.g. see Figure 2).

Determination of coordinates of coal samples specific components was carried out using two types of microscopes. Microscope operating in transmitted light was used to allocate the coordinates for the path of the indenter movement on the motorized table of automated depth-sensing nanoindentation system. Accuracy in setting the area of the indentation was confirmed by microscope, operating in reflected light. Experiments were carried out on the installation Hysitron TriboIndenter (Hysitron Inc., Minneapolis, MN) at room temperature, using a diamond triangular Berkovich pyramidal indenter whose tip radius was estimated as 250 nm.

Mechanical properties of the specific components of coal samples were evaluated within the 100x100 μm highlighted domain with a square grid (ten by ten). Distance between the grid points was 10 microns. Presence of such a large number of indentation points allowed to generate local maps of mechanical properties and, consequently, to determine trends in the experimental data variation, and identify the impact of edge effects. It also provided statistically significant characteristics of the tested area.

We used two protocols for finding curves for load dependence on time. The load-time dependences were either triangular or trapezoidal with 2 seconds delay at maximum load. Last protocol allowed estimating the viscoelastic characteristics of the individual components of the tested macerals groups. The pile-up phenomena that may occur during the experiments was excluded by specifically adjusting the load-displacement range (pile-up is minimised at lower penetration) and confirmed by on-line AFM imaging of the sample surface after indentation with the same tip that made the indent.

3.4. Results of experiments

Experiments demonstrated that N14 (the Donetsk coal basin) sample of coal has average hardness values of 408 ± 24 MPa for macerals of liptinite group and 538 ± 61 MPa for vitrinite; the effective contact moduli for the same components at 300 nm maximum depth of indentation were 4.57 ± 0.02 GPa and 5.5 ± 0.3 GPa, respectively (see Figure 3).

There was no significant difference between the results, obtained by two different test protocols (controlled load and displacement). However, data from the controlled movement protocol slightly exceeded those of a controlled load, possibly due to a greater penetration depth. Measurements of hardness and elastic modulus have not demonstrated any systematic variations across the domain of the indentation for each component. This indicates that during the experiment there were no effects of inclination or boundary effects at the received data. The domain occupied by inertinite showed small variations of data. Note that these domains were extremely small. In some cases we observed firmer and more rigid parts within the grid of indentation points. This effect can be explained by the presence of inorganic particles in the coal sample. This led to greater variation within the contact module (6.4 ± 1.4 GPa) and hardness (477 ± 203 MPa) of measured values.

For a sample N5 (the Kizel coal basin) in the vitrinite maceral zone the experimentally determined average values of hardness *H*, the contact module and the maximum depth of the indentation (h_{max}) at maximum load are presented in Table 1.

Table 1. Average measured values of vitrinite mechanical properties (Kizel coal basin)

Type of load	Contact modulus, GPa	Hardness, MPa	Average maximal penetration depth, nm
Triangular	5.48±1.07	367±105	300±43
Trapezoidal	5.31±1.1	387±134	295±49

For the area of inertinite (of the same sample) the average measured values at the maximum load are shown in Table 2.

Table 2. Average measured values of inertinite mechanical properties (Kizel coal basin)

Type of load	Contact modulus, GPa	Hardness, MPa	Average maximal penetration depth, nm
Triangular	5.37±1.21	303±126	329±13
Trapezoidal	5.89±2.0	349±150	292±88

Graphically the above results are shown in Figure 4.

4. Statistical analysis of the fitness of approximating functions

The above-mentioned numerical values of contact moduli were calculated using the common Oliver-Pharr interpretation of BASh-dependence [20]. However, the values of the contact moduli obtained from the slope of the upper part of the $P-h$ unloading branch are not the true values for the sample, and represent equivalent moduli E_{eq}^{*} of the section/substrate system. In order to obtain the actual values of elastic moduli of sample, one should use the methods discussed in [34-36].

In particular, the glue may be considered as an elastic base with an exponentially decreasing function of influence. Some uncertainty in the determination of the contact moduli of different group's macerals, obtained by BASh formula and the Oliver and Pharr approach, may be explained by the fact that the approach has been developed for a homogeneous elastic half-space.

To estimate the true elastic moduli of specific components of the coal films, we have performed nanoindentation experiments with varying maximum depth of indentation (see Figures 5 - 8), and studied the fitness of various approximating functions. Here we provide the results of fitting for only two coal macerals, namely vitrinite and inertinite. This choice is reasoned by our observations that vitrinite components were very viscoelastic, whereas inertinite ones showed relatively larger stiffness in comparison with the other macerals (liptinite and vitrinite).

There are many statistical tools for validation of an approximation [37, 38]. To find the extent to which the resulting function fits the experimental data, we estimated the coefficient of determination and the residual sum of squares. The coefficient of determination R^2 indicates the degree of statistical dependence of values approximating the true function on the sample data (in our case these are the experimental values), i.e. roughly speaking, R^2 indicates the fraction of the total variability that is accounted for by the approximating function. The closer the coefficient

of determination is to 1, the higher the quality of the approximating function. Usually R^2 is calculated by the following formula:

$$R^2 = 1 - \frac{\sum_{i=1}^{N}(y_i - f(x_i, \bar{b}))^2}{\sum_{i=1}^{N}(y_i - y_i)^2},$$

where y_i is true value of approximated quantities, $f(x_i, \bar{b})$ are the values obtained using a model (function) at the relevant points, $\bar{b}$ is a set of adjustable parameters of function $f(x_i, \bar{b})$, y_i are average values of sampling, *N* - number of quantities in the sampling.

The residual sum of squares *RSS* is calculated as the sum of squared deviations of experimental data from the approximating function

$$RSS = \sum_{i=1}^{N}(y_i - f(x_i, \bar{b}))^2 .$$

The closer *RSS* to zero, the higher the degree of approximation of the experimental data presented by function.

We have considered the approximating functions, presented in literature, for evaluating values of elastic contact moduli of samples during nanoindentation. For the selection of the fitting parameters of functions, we used Matlab software package with Curve Fitting Toolbox add-on, which is one of the most powerful tools of mathematical analysis of data for selection parameters of the approximating functions, including manual regime. The add-on allows the regression analysis based on a nonlinear least squares method. It is to minimize the *RSS* function over the set of parameters $\bar{b}$. The solution is found by minimizing the problem through numerical differentiation of *RSS* = *RSS*($\bar{b}$) for each of the parameters and solutions of the following system of equations

$$\sum_{i=1}^{N}(y_i - f(x_i, \bar{b}))\frac{\partial f(x_i, \bar{b})}{\partial b} = 0,$$

where $b \in \bar{b}$.

As it was mentioned above, many different types of relationship (4) have been proposed for the dependence of the equivalent modulus of the film - substrate (glue) system on the maximum depth of indentation. An excellent review of such dependencies was presented by Menčík et al [34]. In addition, Jung et al. [35] proposed the following empirical formula:

$$E^*_{eq}(h) = E^*_s\left(E^*_f / E^*_s\right)^L, \quad L = 1/[1 + A(h/t)^C], \tag{5}$$

where A and C are adjustable parameters, determined from experimental conditions and inverse problem of data approximation.

Solution of the inverse problem for the formula (5) has shown that the best fit of the experimental data by Yung's function (5) is obtained by the following expressions

$$E^*_{eq}(h) = 2(21/2)^L, \quad L = 1/[1 + 2414.32(h/t)^{1.94}], \tag{6}$$

and

$$E^*_{eq}(h) = 2(70/2)^L, \quad L = 1/[1 + 5017.72(h/t)^{1.94}] \tag{7}$$

the vitrinite and inertinite components respectively.

One of the authors (FB) suggested the following approximating function that is also based on the use of power-law relation

$$E^*_{eq}(h) = E^*_s + \left(E^*_f - E^*_s\right)\left[1 - h/t\right]^{-\alpha} \quad , \tag{8}$$

where $\alpha > 0$ is an adjustable parameter. Perhaps the expression (8) has been used by someone earlier because its form is very simple; however, we are not aware about such works.

Using the Borodich power-law dependence (8), the following equality is obtained for the best fit of the experimental results on vitrinite components

$$E^*_{eq}(h) = 2 + (20.28 - 2)\left[1 - h/t\right]^{-1166} \quad . \tag{9}$$

Analogously, for the experiments on inertinite we have

$$E^*_{eq}(h) = 2 + (27.69 - 2)\left[1 - h/t\right]^{-82.3} \quad . \tag{10}$$

The following Perriot-Barthel function [36] may be also used to fit the data

$$E^*_{eq}(h) = E^*_s + \frac{E^*_f - E^*_s}{1 + (x_0\, t/h)^n}, \tag{11}$$

where parameters x_0 and n are to be evaluated. Here, x_0 corresponds to the t/h value of the relation at which $E^*_{eq} = \dfrac{E^*_f + E^*_s}{2}$. Using (11), we have found that the results of tests of vitrinite components may be fitted by

$$E^*_{eq}(h) = 2 + \frac{65 - 2}{1 + (0.006\, t/h)^{-2.37}}, \tag{12}$$

and the results of tests of the intertinite components by

$$E^*_{eq}(h) = 2 + \frac{27 - 2}{1 + (0.01\, t/h)^{-2.16}}. \tag{13}$$

One of the most appropriate functions describing the dependence of E^*_{eq} on the maximum depth of the indentation is the exponential function [34], i.e. the approximating function is $\Phi(x) = e^{-\alpha x}$, where $\alpha > 0$ is an adjustable parameter. We have found that the best fit of the data by the exponential approximating function

$$E^*_{eq}(x) = E^*_S + (E^*_f - E^*_S)e^{-\alpha(h/t)}. \ , \tag{14}$$

is observed by the following expressions

$$E_{eq}^{*}(x) = 2 + (21.56 - 2)e^{-30.23x}, \tag{15}$$

and

$$E_{eq}^{*}(x) = 2 + (26.91 - 2)e^{-30.31x}. \tag{16}$$

for the vitrinite and inertinite components respectively.

A linear approximating function was also discussed in [34] for $x = h/t$

$$E_{eq}^{*}(x) = E_f + (E_S - E_f)x.$$

Using the above approximating function, we have got the following expressions of the best fit

$$E_{eq}^{*}(x) = 5.65 + (2 - 5.65)x, \tag{17}$$

and

$$E_{eq}^{*}(x) = 5.48 + (2 - 5.73)x. \tag{18}$$

for the vitrinite and inertinite components respectively.

Doerner and Nix [29] introduced another type of empirical relation that is similar to (14), however the moduli are replaced by their reciprocals

$$\frac{1}{E_{eq}^{*}(x)} = \frac{1}{E_f} + \left(\frac{1}{E_s} - \frac{1}{E_f}\right)e^{-\alpha/x}, \tag{19}$$

where α is an adjustable parameter. Using (19), we get the following expressions of the best fit

$$\frac{1}{E_{eq}^{*}(x)} = \frac{1}{25} + \left(\frac{1}{2} - \frac{1}{25}\right)e^{-0.07/x}, \tag{19}$$

and

$$\frac{1}{E_{eq}^{*}(x)} = \frac{1}{27} + \left(\frac{1}{2} - \frac{1}{27}\right)e^{-0.07/x}. \tag{20}$$

for the vitrinite and inertinite components respectively.

The use of the reciprocal exponential function [34]

$$\frac{1}{E_{eq}^{*}(x)} = \frac{1}{E_s} + \left(\frac{1}{E_f} - \frac{1}{E_s}\right)e^{-\alpha x}. \tag{21}$$

gave the following expressions for the best fit of the experimental data

$$\frac{1}{E_{eq}^{*}(x)} = \frac{1}{2} + \left(\frac{1}{19} - \frac{1}{2}\right)e^{-6.49x}, \tag{22}$$

and

$$\frac{1}{E^*_{eq}(x)} = \frac{1}{2} + \left(\frac{1}{28} - \frac{1}{2}\right) e^{-6.20x}, \tag{23}$$

for the vitrinite and inertinite components respectively.

All the obtained approximating curves are shown in Figures 5 and 7, 6 and 8 (for the domains occupied by the vitrinite and inertinite, respectively). The values of the coefficient of determination and the residual for the above approximation functions are given in Table 3.

Table 3. Statistical characteristics of approximating functions

Approximating function	Vitrinite		Internite	
	Coefficient of determination	Residual	Coefficient of determination	Residual
Power-law (Yung et al.)	0.95	2.49	0.84	9.52
Perriot-Barthel	0.95	2.52	0.837	9.53
Exponential	0.94	2.40	0.84	9.56
Power-law (Borodich)	0.94	2.44	0.83	9.56
Linear	0.045	53.48	0.069	55.38
Doerner and Nix	0.84	8.99	0.81	10.84
Reciprocal exponential	0.64	20.1	0.69	18.03

The statistical characteristics of performance of the approximating functions are shown in Table 3. It should also be noted that there exists a large variation in the values found for the elastic modulus E^*_f (Table 4).

Table 4. Elastic modulus values found by the approximating functions

Approximating function	Elastic modulus E^*_f, GPa	
	Vitrinite	Inertinite
Power-law (Yung)	21	70
Perriot-Barthel	65	27
Exponential	21.56	26.91
Power-law (Borodich)	20.28	27.69
Linear	5.65	5.73
Doerner and Nix	25	27
Reciprocal exponential	19	28

The additional microbrittleness experiments showed that the mismatch between the true values of elastic moduli of the macerals is not very significant. Our comparison of the results for each of the macerals groups obtained by all considered approximation has shown that one can expect that the true value of the reduced modulus for inertinite is within the interval from 22.69 GPa to 28 GPa and for vitrinite it is within the interval from 19 GPa to 28 GPa. Analysis of the statistical characteristics of approximating functions (see. Table 3) showed that the accuracy of the selection of adjustable parameters is at approximately the same level for the first four functions, however the last three, namely the linear function, Doerner and Nix and reciprocal exponential function, have shown much lower values of statistical significance (see also Figures 5 and 6. Therefore, we can conclude that the elastic contact modules are approximately 21 GPa

for vitrinite and 27 GPa for inertinite, and the most appropriate approximating functions are the exponential function (14) and the function proposed in this paper (8). The conclusions are based on the analysis of statistical characteristics and values of the elastic moduli.

5. Conclusion

It has been argued that the microindentation standard methods are not effective for the study of mechanical properties of materials that have the characteristic scale of spatial inhomogeneity at the micrometer range. To study mechaniucal properties of specific components of such materials, it is proposed to prepare very thin films of the materials, and to employ a combination of the depth-sensing nanoindentation techniques along with optical microscopy methods.

Taking coal as an example of such materials, it was shown that, in order to minimize the impact of internal pores and cracks in the samples of coal, it is the most informative to use DSNI at the coal petrographic thin sections with thickness of 10-20 microns.

Some experimental results of depth-sensing indentation are presented. The use of coal films with the thickness of 13-14 microns gives an additional advantage: the thin sections are transparent and therefore, they can be studied by optical microscopy with transmitted light, which allows us to determine accurately the type of the component of coal sample and to set the coordinates of their location during the automatic stage of experiment.

We studied mechanical characteristics of the various coal macerals, and revealed a significant influence of the glue layer on the obtained experimental data. To take into account this influence, we considered seven different types of approximating functions allowing the extraction of the true elastic moduli of the samples. Using statistical approach, it has been shown that a number of popular approximating functions do not accurately allocate the true elastic moduli of thin coal sections. An analysis of the appropriateness of the functions for our specific data was based on a comparison of the statistical characteristics of approximation and the values of elastic contact moduli obtained from the samples. We found that the most appropriate approximating functions are: exponential function (14) and the function (8) proposed in this work.

Acknowledgments

The work was supported by Russian Science Foundation grant (project #16-17-10217).

REFERENCES

1. M.M. Khrushchov, E.S. Berkovich, Experience in the application of electronic microscope for measurement of very small imprints obtained at microhardness test, Izv. AN SSSR. Otd. Tekh. Nauk. (1950) 1645–1649. (Russian)
2. B.W. Mott, Micro-indentation hardness testing /B. W. Mott, Butterworth, London, 1956.
3. M.-C.G. Klein, S.N. Gorb, Epidermis architecture and material properties of the skin of four snake species, J. R. Soc. Interface. 9 (2012) 3140–3155. doi:10.1098/rsif.2012.0479.
4. D. Carnelli, P. Vena, M. Dao, C. Ortiz, R. Contro, Orientation and size-dependent mechanical modulation within individual secondary osteons in cortical bone tissue, J. R. Soc. Interface. 10 (2013) 20120953–20120953. doi:10.1098/rsif.2012.0953.
5. GOST 21206-75 Coals and anthracite. Determination method for microhardness and microbrittleness, 1975. USSR State Committee on Standards.
6. M.A. Iofis, A.I. Shmelev, Engineering Geomechanics at Underground Developments, Nedra, Moscow, 1985. (Russian)

7. S.A. Epshtein, O. V. Barabanova, V.I. Minaev, J. Weber, D.L. Shirochin, Effect of dimethylformamide treatment of coals on their thermal degradation and elastic-plastic properties, Solid Fuel Chem. 41 (2007) 210–215. doi:10.3103/S0361521907040052.
8. S.A. Epshtein, Physical and mechanical properties of the coal vitrinites of the different genotypes, Min. Informational Anal. Bull. (2009) 58–69.
9. S.A. Musyal, Microhardness and microbrittleness as possible parameters for classification of fossil coals, in: I.I. Amnosov (Ed.), Petrogr. Specif. Prop. Coals, USSR Academy of Sciences Publisher, Moscow, 1963: pp. 164–188.
10. K. Velez, S. Maximilien, D. Damidot, G. Fantozzi, F. Sorrentino, Determination by nanoindentation of elastic modulus and hardness of pure constituents of Portland cement clinker, Cem. Concr. Res. 31 (2001) 555–561. doi:10.1016/S0008-8846(00)00505-6.
11. G. Constantinides, F.-J. Ulm, K. Van Vliet, On the use of nanoindentation for cementitious materials, Mater. Struct. 36 (2003) 191–196. doi:10.1617/14020.
12. W. Zhu, J.J. Hughes, N. Bicanic, C.J. Pearce, Nanoindentation mapping of mechanical properties of cement paste and natural rocks, Mater. Charact. 58 (2007) 1189–1198. doi:10.1016/j.matchar.2007.05.018.
13. H. Ban, P. Karki, Y.-R. Kim, Nanoindentation Test Integrated with Numerical Simulation to Characterize Mechanical Properties of Rock Materials, J. Test. Eval. 42 (2014) 20130035. doi:10.1520/JTE20130035.
14. S. Nemat-Nasser, M. Hori, Micromechanics: Overall properties of heterogeneous materials, North-Holland. 1999.
15. F.M. Borodich, S.J. Bull, S.A. Epshtein, Nanoindentation in Studying Mechanical Properties of Heterogeneous Materials, ISSN J. Min. Sci. 51 (2015) 1062–7391. doi:10.1134/S1062739115030072.
16. F.M. Borodich, L.M. Keer, Contact problems and depth-sensing nanoindentation for frictionless and frictional boundary conditions, Int. J. Solids Struct. 41 (2004) 2479–2499. doi:10.1016/j.ijsolstr.2003.12.012.
17. F.M. Borodich, Contact problems at nano/microscale and depth sensing indentation techniques, Mater. Sci. Forum. 662 (2010) 53–76. doi:10.4028/www.scientific.net/MSF.662.53.
18. G.N. Kalei, Some results of microhardness test using the depth of impression, Mashinovedenie. 4 (1968) 105–107. (Russian).
19. M.M. Khrushchov, E.S. Berkovich, Experience in the application of electronic microscope for measurement of very small imprints obtained at microhardness test, Izv. AN SSSR. Otd. Tekh. Nauk. (1950) 1645–1649. (Russian)
20. S.J. Bull, Nanoindentation of coatings, J. Phys. D Appl. Phys. 38 (2005) 393–413. doi:10.1088/0022-3727/38/24/R01.
21. I.I. Argatov, F.J. Sabina, Small-scale indentation of an elastic coated half-space: The effect of compliant substrate, Int. J. Eng. Sci. 104 (2016) 87–96. doi:10.1016/j.ijengsci.2016.04.008.
22. S.I. Bulychev, V.P. Alekhin, M.K. Shorshorov, A.P. Ternovskij, G.D. Shnyrev, Determination of Young modulus by the hardness indentation diagram, Zavod. Lab. 41 (1975) 1137–1140.
23. J. Menčík, Determination of mechanical properties by instrumented indentation, Meccanica. 42 (2007) 19–29. doi:10.1007/s11012-006-9018-6.
24. B.A. Galanov, Approximate solution of some contact problems with an unknown contact area under conditions of power law of material hardening, Dopovidy Akad. Nauk Ukr. RSR, Ser. A. (1981) 35–40. (Russian and Ukrainian)

25. B.A. Galanov, O.N. Grigor'ev, Y. V Milman, I.P. Ragozin, Determination of the hardness and Young's modulus from the depth of penetration of a pyramidal indenter, Strength Mater. 15 (1983) 1624–1628.
26. F.M. Borodich, L.M. Keer, Evaluation of elastic modulus of materials by adhesive (no-slip) nano-indentation, Proc. R. Soc. A Math. Phys. Eng. Sci. 460 (2004) 507–514. doi:10.1098/rspa.2003.1224.
27. F.M. Borodich, The Hertz-Type and Adhesive Contact Problems for Depth-Sensing Indentation, in: Adv. Appl. Mech., 2014: pp. 225–366. doi:10.1016/B978-0-12-800130-1.00003-5.
28. S.A. Epshtein, F.M. Borodich, S.J. Bull, Evaluation of elastic modulus and hardness of highly inhomogeneous materials by nanoindentation, Appl. Phys. A Mater. Sci. Process. 119 (2015) 325–335. doi:10.1007/s00339-014-8971-5.
29. M.F. Doerner, W.D. Nix, A method for interpreting the data from depth-sensing indentation instruments, J. Mater. Res. 4 (1986) 601–609. doi:10.1017/CBO9781107415324.004.
30. A.D. Kerr, Elastic and Viscoelastic Foundation Models, J. Appl. Mech. 31 (1964) 491–498. doi:10.1115/1.3629667.
31. V.I. Kuznetsov, Elastic foundation, Literature on construction and architecture publishing, Moscow, 1952. (Russian)
32. K. Wieghardt, Über den Balken auf nachgiebiger Unterlage, ZAMM - Zeitschrift Für Angew. Math. Und Mech. 2 (1922) 165–184. doi:10.1002/zamm.19220020301.
33. M.M. Filonenko-Borodich, Some approximate theories of the elastic foundation, Uchenye Zap. Mosk. Gos. Univ. Mekhanika. 46 (1940) 3–18. (Russian)
34. J. Menčík, D. Munz, E. Quandt, E.R. Weppelmann, M. V. Swain, Determination of elastic modulus of thin layers using nanoindentation, J. Mater. Res. 12 (1997) 2475–2484. doi:10.1557/JMR.1997.0327.
35. Y.G. Jung, B.R. Lawn, M. Martyniuk, H. Huang, X.Z. Hu, Evaluation of elastic modulus and hardness of thin films by nanoindentation, J. Mater. Res. 19 (2004) 3076–3080. doi:10.1557/JMR.2004.0380.
36. A. Perriot, E. Barthel, Elastic contact to a coated half-space: Effective elastic modulus and real penetration, J. Mater. Res. 19 (2004) 600–608. doi:10.1557/jmr.2004.19.2.600.
37. M.R. Spiegel, Schaum's Outline of Theory And Problems Of Probability And Statistics, McGraw-Hill, New York, 1975.
38. N. Draper, H. Smith, Applied Regression Analysis, Wiley, 1998.

List of Figures captions

Figure 1 A reflected light microscope view of a thin section of a coal sample.

Figure 2. Colour image of coal sample in transmitted light (vitrinite components have red colour, liptinite is yellow, and inertinite is black).

Figure 3. Colour image of coal sample N14 (Donetsk coal basin) in transmitted light. Vitrinite has red colour, liptinite is orange, and inertinite is black. Maximal load was 10 mN.

Figure 4. Colour image of coal sample N5 (Kizel coal basin) in transmitted light. Vitrinite has brown colour, inertinite is black, liptinite is yellow. Relatively homogeneous zones of vitrinite are resilient and viscoelastic. Areas of inertinite are relatively harder and do not demonstrate viscoelastic properties.

Figure 5. Experimental relation between equivalent contact modulus E_{eq}^{*} and the maximum indentation depth h for vitrinite macerals of coal sample N5.

Figure 6. Experimental relation between equivalent contact modulus E_{eq}^{*} and the maximum indentation depth h for inertinite macerals of coal sample N5.

Figure 7. Experimental results and their approximations for less efficient approximation functions. The relation between equivalent contact modulus E_{eq}^{*} and the maximum indentation depth h for vitrinite macerals of coal sample N5.

Figure 8. Experimental results and their approximations for less efficient approximation functions. Experimental relation between equivalent contact modulus E_{eq}^{*} and the maximum indentation depth h for inertinite macerals of coal sample N5.

Figure 1 A reflected light microscope view of a thin section of a coal sample.

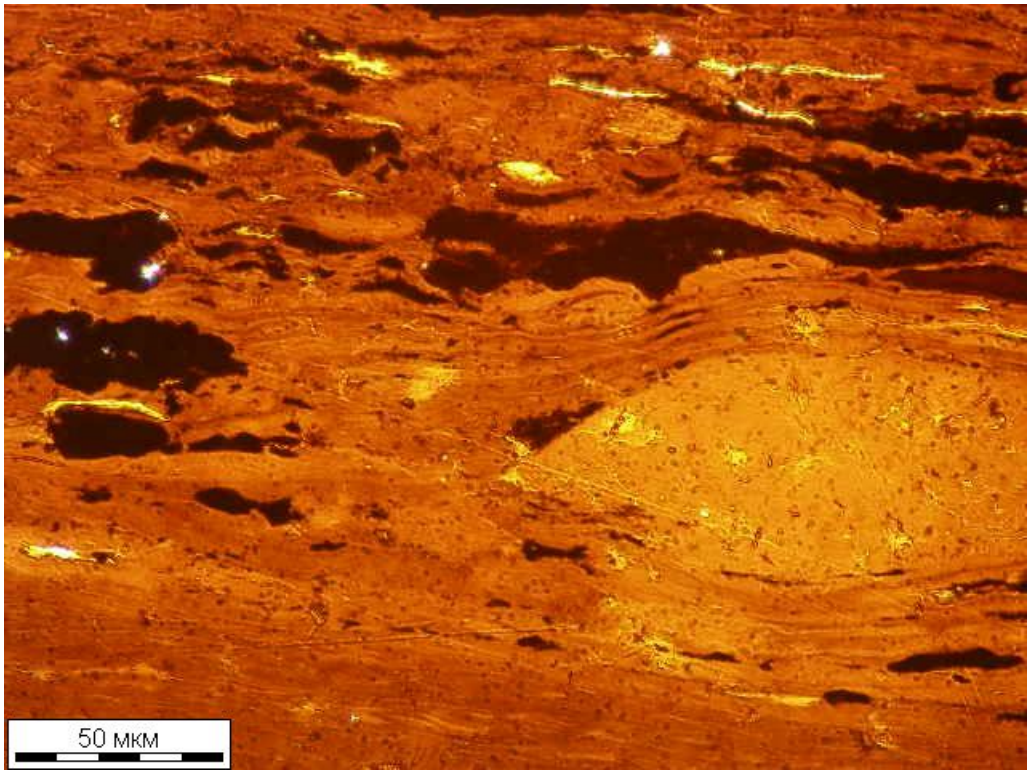

Figure 2. Colour image of coal sample in transmitted light (vitrinite components have red colour, liptinite is yellow, and inertinite is black).

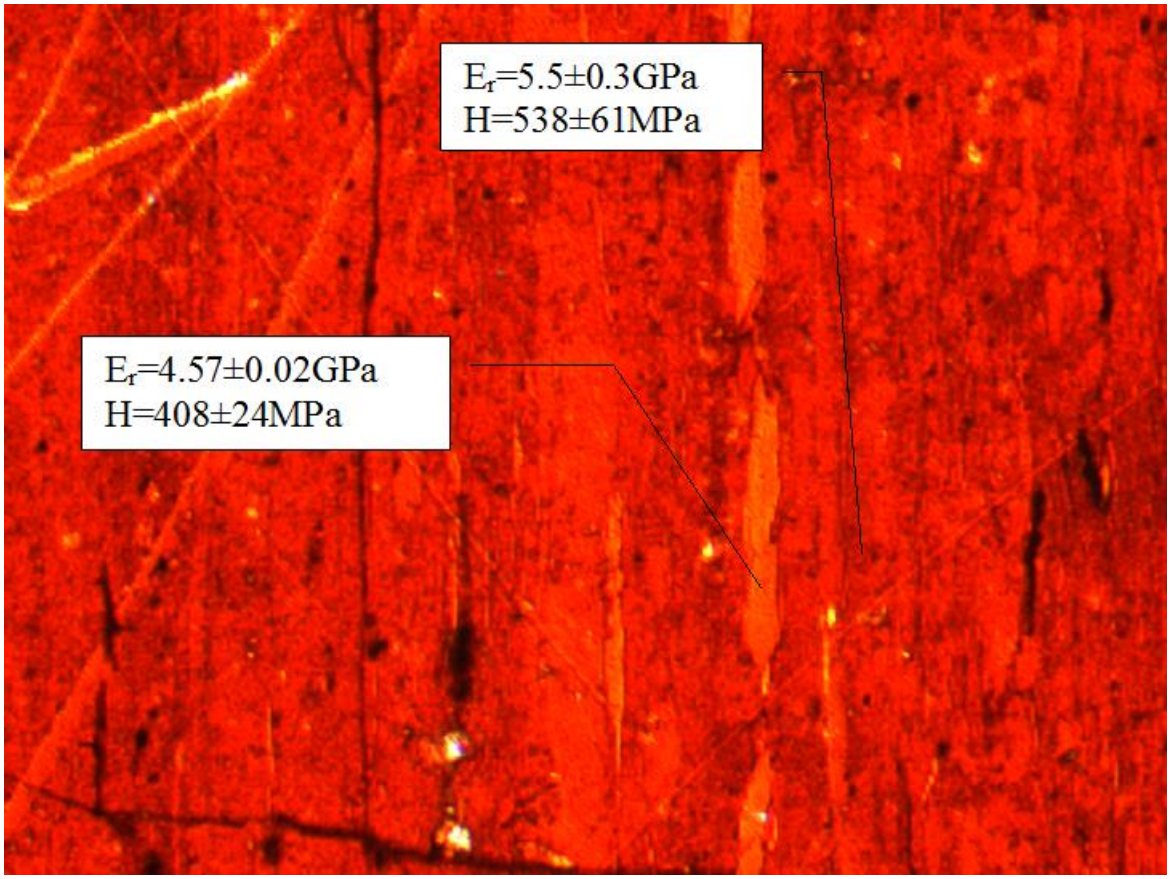

Figure 3. Colour image of coal sample N14 (Donetsk coal basin) in transmitted light. Vitrinite has red colour, liptinite is orange, and inertinite is black. Maximal load was 10 mN.

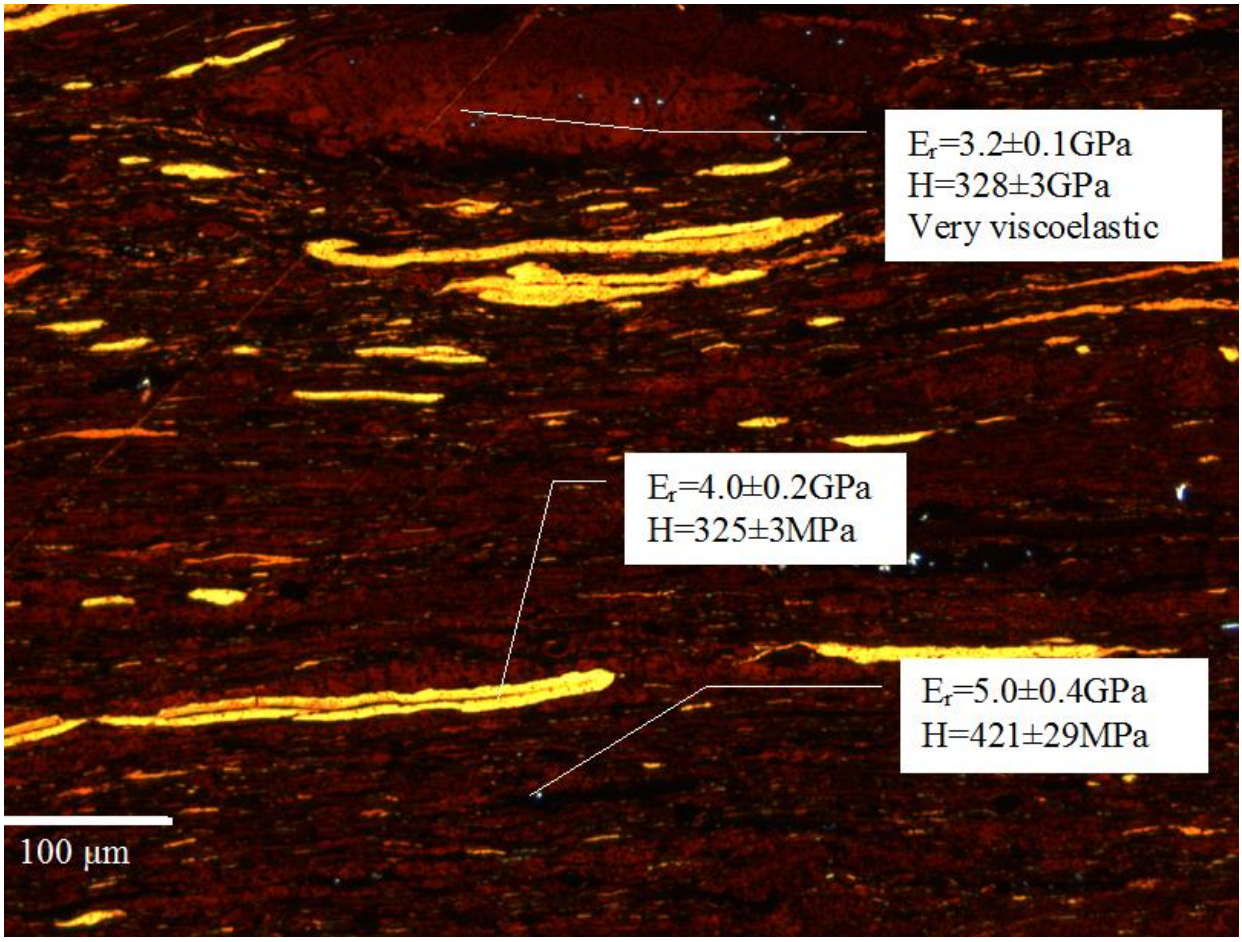

Figure 4. Colour image of coal sample N5 (Kizel coal basin) in transmitted light. Vitrinite has brown colour, inertinite is black, liptinite is yellow. Relatively homogeneous zones of vitrinite are resilient and viscoelastic. Areas of inertinite are relatively harder and do not demonstrate viscoelastic properties.

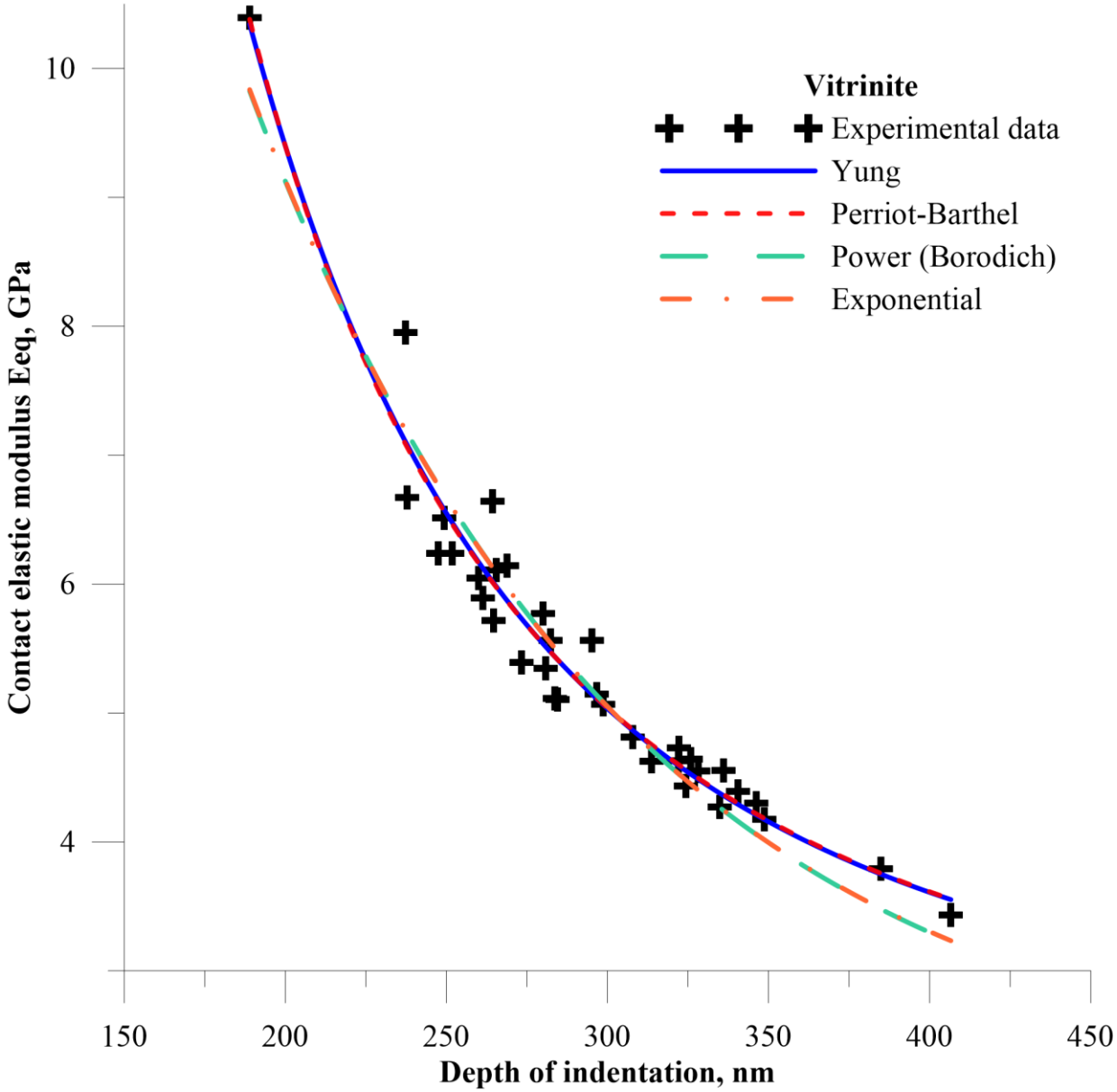

Figure 5. Experimental relation between equivalent contact modulus E_{eq}^{*} and the maximum indentation depth h for vitrinite macerals of coal sample N5.

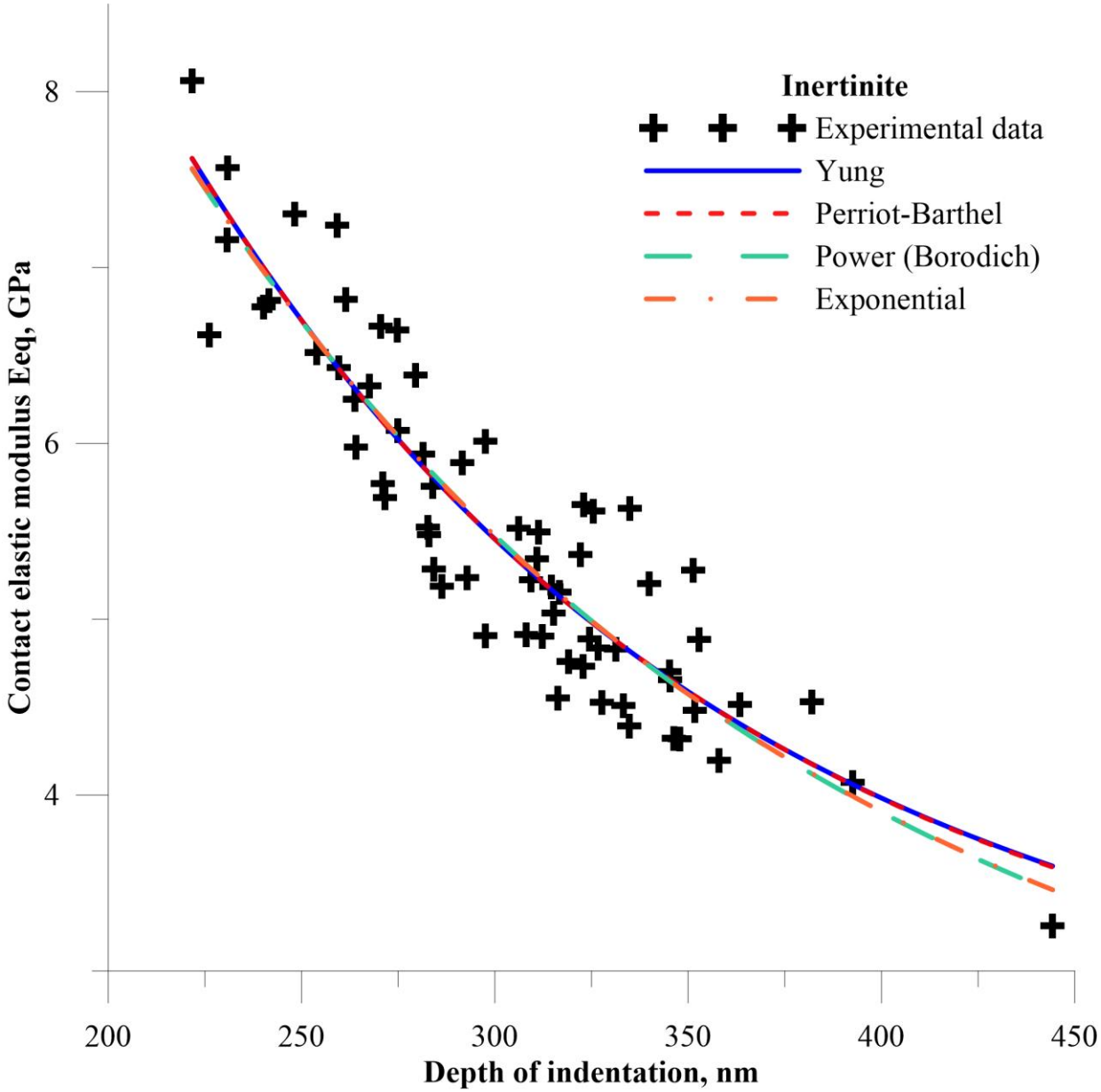

Figure 6. Experimental relation between equivalent contact modulus E^*_{eq} and the maximum indentation depth h for inertinite macerals of coal sample N5.

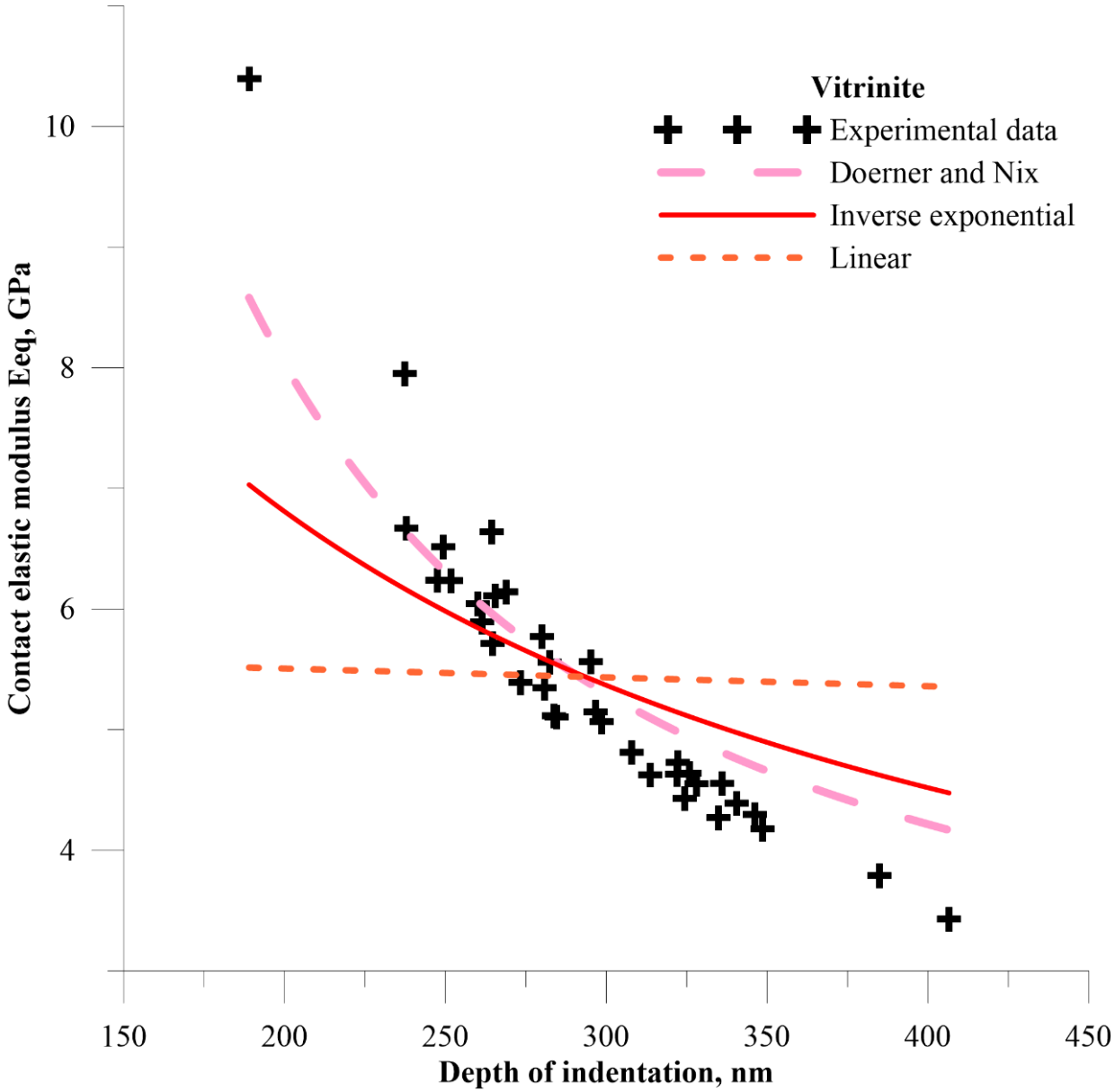

Figure 7. Experimental results and their approximations for less efficient approximation functions. The relation between equivalent contact modulus E_{eq}^{*} and the maximum indentation depth h for vitrinite macerals of coal sample N5.

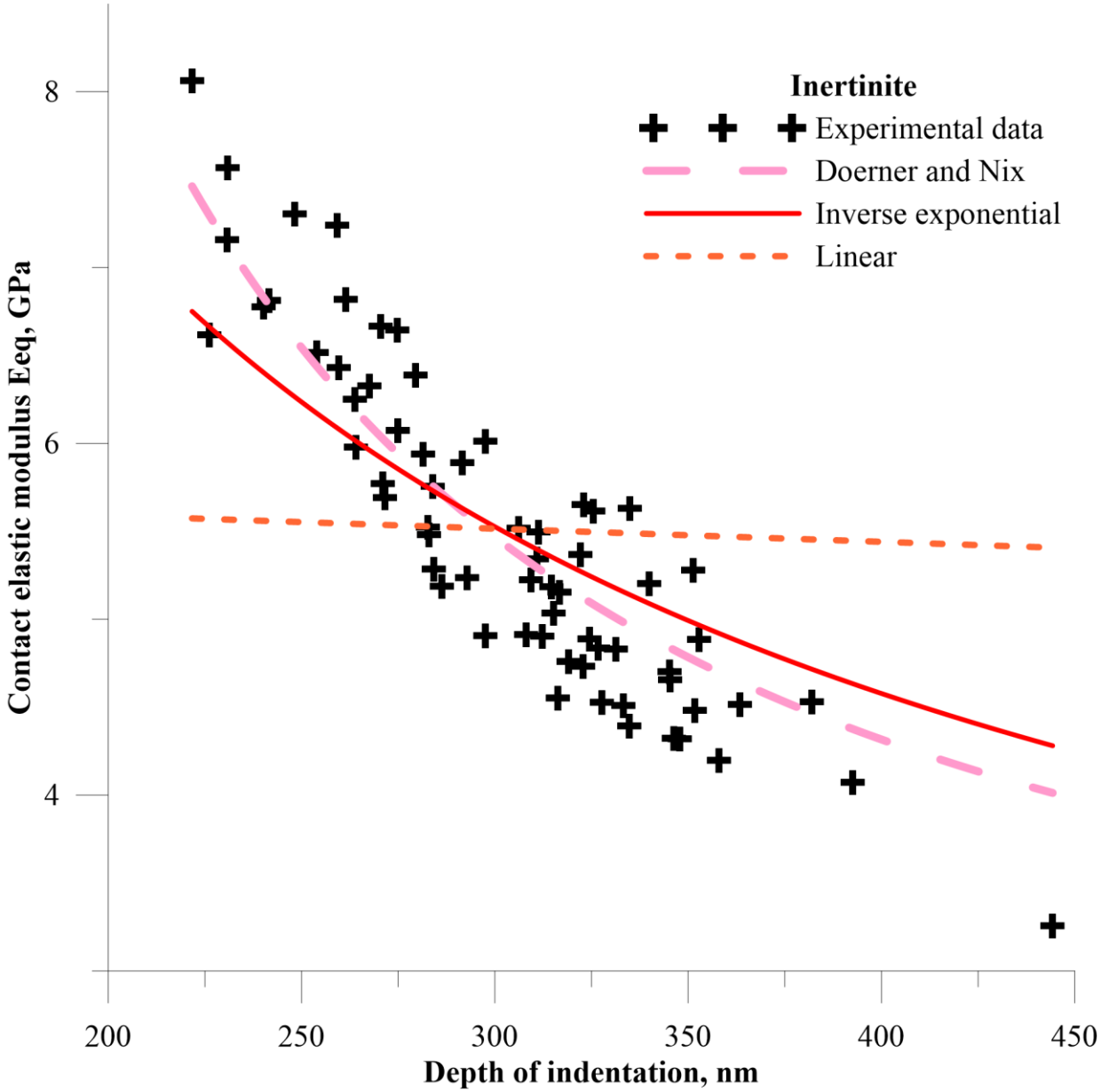

Figure 8. Experimental results and their approximations for less efficient approximation functions. Experimental relation between equivalent contact modulus E^*_{eq} and the maximum indentation depth h for inertinite macerals of coal sample N5.